

# Multidisciplinary inferences on a newly recognized active east-dipping extensional system in Central Italy

Giusy Lavecchia,<sup>1</sup> Guido Maria Adinolfi,<sup>2</sup> Rita de Nardis,<sup>1,3</sup> Federica Ferrarini,<sup>1</sup> Daniele Cirillo,<sup>1</sup> Francesco Brozzetti,<sup>1</sup> Raffaella De Matteis,<sup>4</sup> Gaetano Festa<sup>2</sup> and Aldo Zollo<sup>2</sup>

<sup>1</sup>CRUST, DiSPUTer, Università “G. d’Annunzio”, Chieti Scalo 66013, Italy; <sup>2</sup>Dipartimento di Fisica “Ettore Pancini”, Università di Napoli Federico II, Naples, Italy; <sup>3</sup>Dipartimento della Protezione Civile, Rome, Italy; <sup>4</sup>Dipartimento di Scienze e Tecnologie, Università degli Studi del Sannio, Benevento, Italy

## ABSTRACT

We use a multidisciplinary approach to gather preliminary evidence for a Quaternary east-dipping extensional detachment in Central Italy. This structure crops out in the Sabini-Eastern Simbruini (SES) and would be hidden at mid-crustal depths beneath the L’Aquila 2009 ( $M_w$ 6.3) epicentral area. The SES geometry is reconstructed through geological mapping, structural analysis and seismic line interpretation. The geometry of the mid-crustal segment, referred to as the Ocre Segment (OS), is interpreted through seismological analyses of the largest aftershock ( $M_w$ 5.4) of the L’Aquila 2009 sequence. The kinematic compatibility

between the SES and the OS under a common SW–NE tensional field is tested through stress inversion of both geological and seismological data. The reliability of OS activation is tested through slip tendency analysis. Like other Italian cases, the SES and the OS are preliminarily interpreted as expressions at different depths of the same unknown east-dipping extensional detachment, characterized by a ramp–flat–ramp geometry.

Terra Nova, 00: 000–000, 2016

## Introduction

The Abruzzo region of Central Italy, struck by the 6 April 2009 L’Aquila earthquake (EQ1,  $M_w$ 6.3), has a high seismic hazard due to well-known west-dipping high-angle seismogenic upper-crustal normal faults (Pace *et al.*, 2006). In contrast to the neighbouring regions of the Northern and Southern Apennines, no east-dipping normal fault system has been determined to be active and/or potentially seismogenic (Fig. 1a).

EQ1 ruptured the SW-dipping Late Quaternary Paganica normal fault from a depth of ~9 km up to the surface and for a length of ~25 km (Boncio *et al.*, 2010; Chiaraluce *et al.*, 2011; Doglioni *et al.*, 2011). Its largest aftershock, which occurred on 7 April (EQ2,  $M_w$ 5.4), nucleated within the Paganica foot-wall rock volume, at a depth of ~14 km (Fig. 1b). In the literature, EQ2 has been associated with a NNW–SSE sub-vertical normal fault (Pino and Di Luccio, 2009; Di Luccio *et al.*, 2010), with an east-dipping low-angle normal fault (Lavecchia *et al.*, 2012), with the extensional

reactivation of an east-dipping Mio-Pliocene thrust (Valoroso *et al.*, 2013) and with a NE-dipping normal fault antithetic to the Paganica fault (Guglielmino *et al.*, 2013). Available EQ2 focal mechanisms (Pondrelli *et al.*, 2010; Scognamiglio *et al.*, 2010; Herrmann *et al.*, 2011; D’Amico *et al.*, 2013) show a high-angle east-dipping plane with a relevant strike-slip component, making the interpretation of the EQ2 seismotectonic context more intriguing.

In this paper, we aim to constrain the fault generating EQ2 and its geometric–kinematic interlinks with the surrounding fault system. By integrating surface and subsurface geology and seismological data, we highlight a previously unrecognized east-dipping extensional system that crops out along the Latium-Abruzzo boundary and possibly released EQ2 at mid-crustal depths.

## Seismotectonic framework

The intermountain Quaternary extensional belt of Central Italy consists of both high-angle (west-dipping) and moderate- to low-angle (east-dipping) normal and normal-oblique faults that cross-cut and offset Mio-Pliocene fold-and-thrust structures and control continental basin growth and earthquake activity (Lavecchia *et al.*, 1994; Doglioni *et al.*, 1999; Ghisetti and

Vezzani, 2002). The west-dipping faults are the best exposed and the most seismogenic (Galadini and Galli, 2000; Boncio *et al.*, 2004; Roberts and Michetti, 2004). Since the last century, they have generated several destructive earthquakes including 1915 Avezzano ( $M_w$ 7), 2009 L’Aquila ( $M_w$ 6.3) and 2016 Central Italy ( $M_w$ 6.5) (Fig. 1a). The east-dipping faults, which have less-evident field expressions, crop out along the western border of the Apennine belt (Boncio *et al.*, 2000; Collettini *et al.*, 2006; Mirabella *et al.*, 2011; Di Naccio *et al.*, 2013; Petricca *et al.*, 2015) and define a regional NNW–SSE fault alignment known as the Etrurian Fault System (EFS; Brozzetti *et al.*, 2009). Crustal transects and earthquake data across the EFS and the Apennines show that the east- and west-dipping normal faults both sole to a common detachment that dips eastward at a low angle to depths of 14–15 km (Barchi *et al.*, 1998; Boncio *et al.*, 2004; Chiaraluce *et al.*, 2007; Eva *et al.*, 2014).

A conceptual scheme of the spatial relationships between the east-dipping detachment and the high-angle antithetic faults is shown in the block diagram of Fig. 1c.

Potentially seismogenic east-dipping normal faults are also located in southern Italy (Fig. 1a), along the ‘Campania-Lucania Extensional Fault System’ (CLEFS in Brozzetti,

Correspondence: Professor Giusy Lavecchia, CRUST, DiSPUTer, Università “G. d’Annunzio”, Chieti Scalo 66013, Italy. Tel.: +39 0871 3556414; e-mail: glavecchia@unich.it

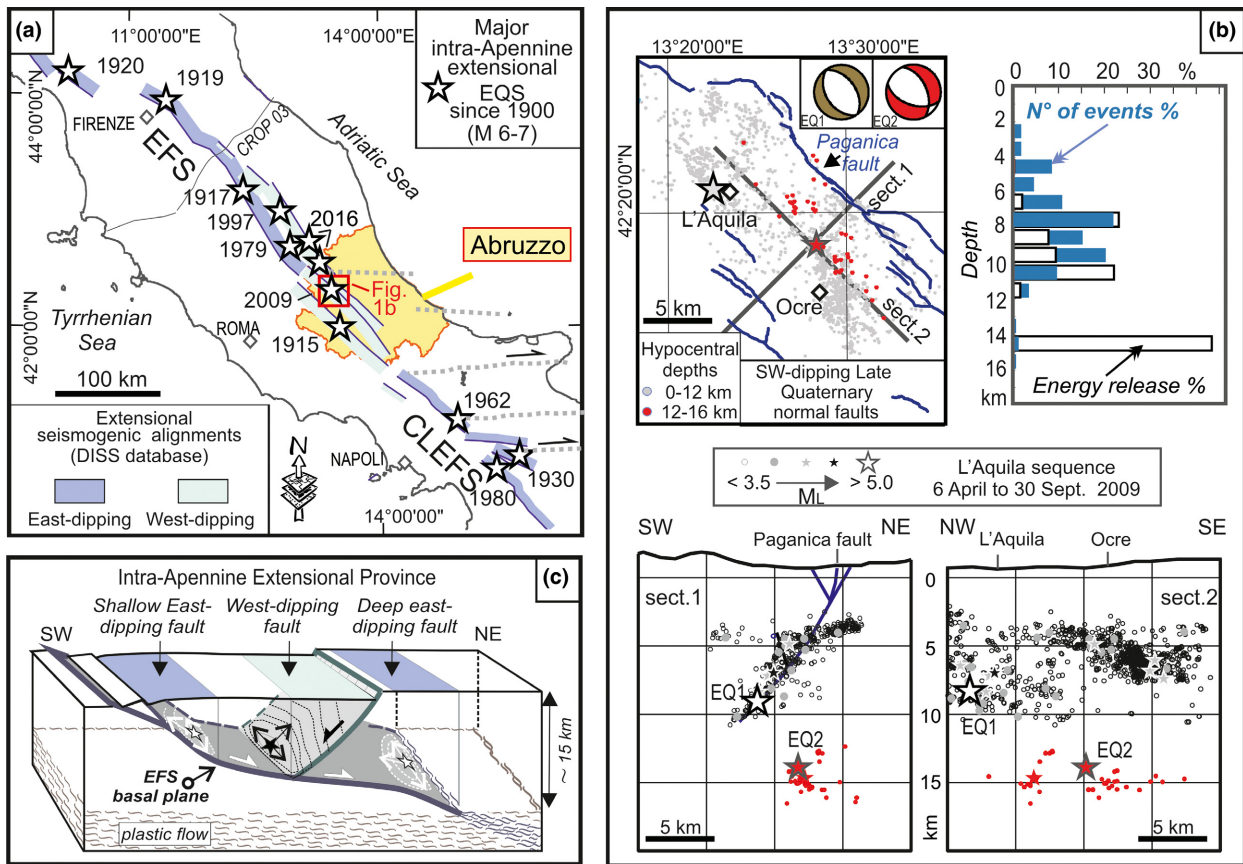


**Fig. 1** Regional and local seismotectonic framework of the L'Aquila 2009 normal fault sequence. (a) Seismogenic composite sources from Working Group DISS (2015) with indications of west- and east-dipping faults of peninsular Italy and of right-lateral strike-slip faults (grey dashed lines) within the Adriatic foreland: EFS = Etrurian Fault System (Brozzetti *et al.*, 2009); CLFES = Campania-Lucania Extensional Fault System (Brozzetti, 2011); stars = major intra-Apennine early-instrumental and instrumental earthquakes (Michele *et al.*, 2016; Rovida *et al.*, 2011). (b) Epicentral and hypocentral distributions (sections 1 and 2) of the L'Aquila sequence (data from Chiaraluce *et al.*, 2011) with the focal mechanisms of the two major events (EQ1 = 6 April,  $M_w$ 6.3; EQ2 = 7 April,  $M_w$ 5.5) (Pondrelli *et al.*, 2010); the histogram highlights the two-layer depth distribution of the aftershock sequence. (c) Sketch of the 3D geometric relationships between the EFS and the antithetic seismogenic high-angle normal faults in Central Italy (Lavecchia *et al.*, 2011). [Colour figure can be viewed at [wileyonlinelibrary.com](http://wileyonlinelibrary.com)]

2011). These faults were first recognized after the 1980 Irpinia normal-fault earthquake ( $M_w$ 6.8); their systematic occurrence is now well accepted (Maschio *et al.*, 2005; De Matteis *et al.*, 2012; Galli and Peronace, 2014). Eastward of the extensional belt, active E–W strike-slip faults are recognized. In instrumental times, they have released moderate earthquakes at mid-crustal depths within the Adriatic foreland (Adinolfi *et al.*, 2015 and references therein).

**EQ2 preferential seismic plane investigation**

With the aim of constraining the preferential seismic plane responsible for EQ2, we first retrieved a new

focal mechanism through Time Domain Moment Tensor (TDMT) full waveform inversion (Dreger and Helmberger, 1993; Dreger, 2003) (Fig. 2a). The obtained focal parameters are given in Table 1, together with data on the quality and stability of the solution. Considering the number of stations and the percentage of double couples, the retrieved solution is reliable and shows a good fit between the synthetic seismograms and the observed data (Fig. S1), as confirmed by uncertainty analysis (Fig. S2). Both nodal planes (N347°/58 and N077°/61) have significant strike-slip components (pitch ~35°); the tensional axis is sub-horizontal and trends SW–NE; the focal mechanism can be classified as

normal-oblique, following the kinematic classification in Zoback (1992).

We performed a kinematic rupture process analysis to model the Apparent Source Time Functions (ASTFs) that were retrieved by the waveform data (Fig. 2b), as developed in Adinolfi *et al.* (2015). The ASTFs were calculated by deconvolution of the impulse response of the medium from the recorded data using the empirical Green's function (EGF) method (Hartzell, 1978) at 15 stations. We selected the 9 April 2009  $M_L$  4.3 aftershock, which occurred at 03:14:53.07 (UTC), as the EGF.

We inverted the ASTFs to obtain a kinematic rupture model using the isochrone back-projection technique (Festa and Zollo, 2006). The method

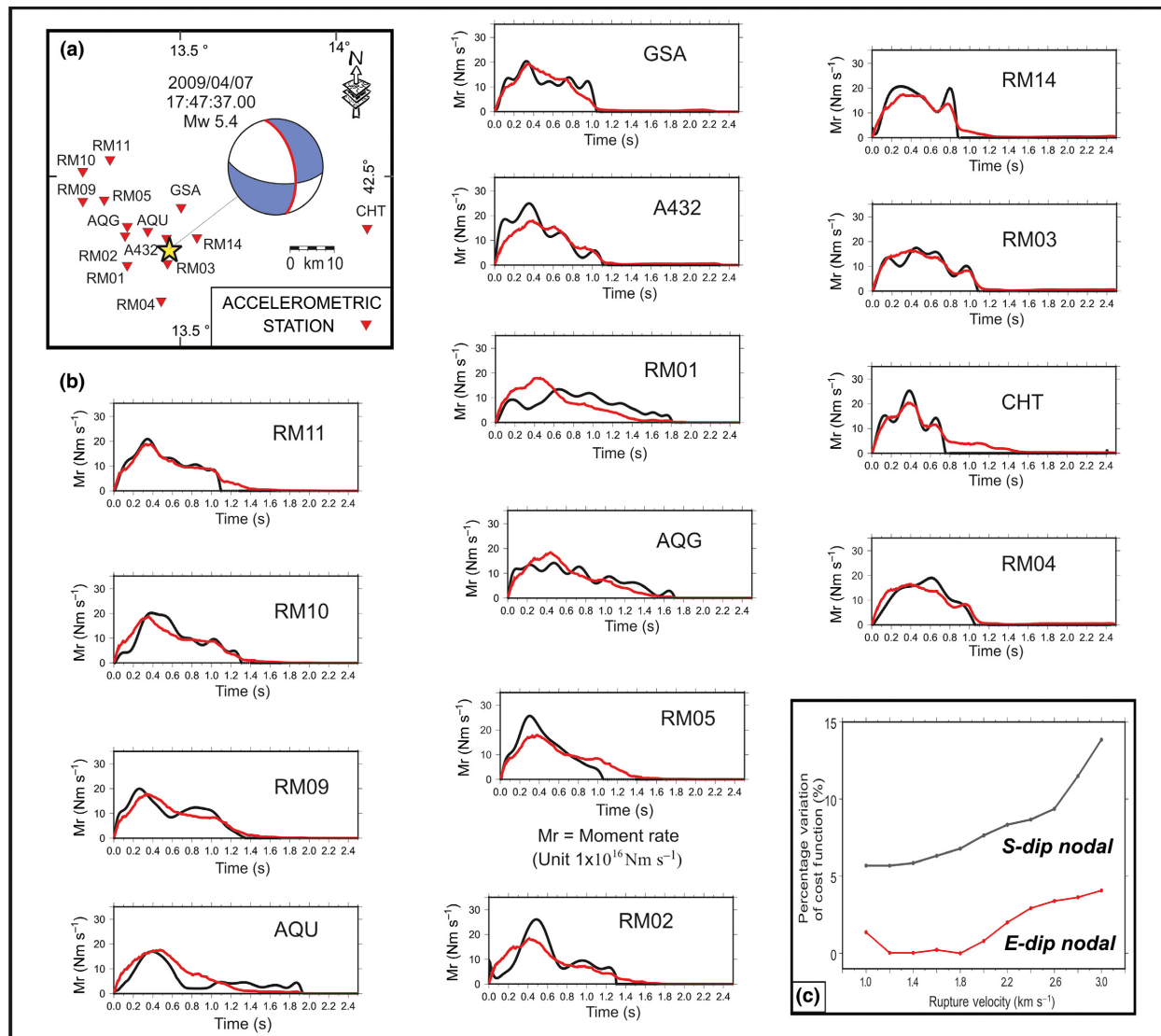


**Fig. 2** Results of the EQ2 seismological analysis. (a) TDMT focal mechanism computation (displacement waveforms in Fig. S1) and seismic station recordings, released by the Centralized National Seismic Network, RSN (Amato and Mele, 2008) and the Italian strong motion network, RAN (Gorini *et al.*, 2010; Zambonelli *et al.*, 2011), used to estimate the Apparent Source Time Functions (ASTFs). (b) Comparison between synthetic (red lines) and observed (black lines) ASTFs for each station used in the analysis. The Moment rate (Mr) unit is  $1 \times 10^{16} \text{ Nm s}^{-1}$ . (c) Percentage variation in the normalized cost function as a function of the rupture velocity for both nodal planes. [Colour figure can be viewed at [wileyonlinelibrary.com](http://wileyonlinelibrary.com)]

back-projects the amplitude of the ASTFs along the isochrones on the fault plane to retrieve the slip distribution that is associated with a single receiver and stacks the retrieved maps to obtain the final slip model.

We investigated the fault plane responsible for the rupture, assuming a constant rupture velocity and comparing the misfit for the two planes indicated by the focal mechanism solution for different values of the rupture velocity ( $1.0\text{--}3.0 \text{ km s}^{-1}$ ).

Fig. 2c shows the difference between the actual misfit function and the misfit value for the minimum that is normalized by this latter value for the fault and auxiliary planes. The east-dipping nodal plane has a curve whose trend is smaller than the misfit for the other plane over the entire range of velocities between 5% and 10%. This result indicates that the ASTFs discriminate the fault plane with a significant reduction in the misfit function. For the east-dipping

plane, the rupture velocity with the minimum misfit is  $1.8 \text{ km s}^{-1}$ . However, the small percentage variation ( $\leq 5\%$ ) of the cost function over the entire range of rupture velocities and the flattening of the function around the minimum indicate a large uncertainty in this parameter.

The ASTF shapes show an initial rapid increase that reveals a small fault dislocation that is relatively confined to a central nucleation zone (Fig. S3).

**Table 1** Moment tensor solutions for the largest aftershock of the 2009 L'Aquila sequence (EQ2), obtained using the TDMT technique; parameters used in the inversion are reported.

Date yyyy/mm/dd	2009/04/07
Origin time hh:mm:ss	17:47:37
$M_w$	5.4
Latitude (°)	42.309
Longitude (°)	13.478
Depth (km)	14.18
Nodal plane1 strike/dip/rake (°)	347/58/-34
Nodal plane2 strike/dip/rake (°)	97/61/-143
$T_{axis}$ Plg/Azi (°)	2/221
$N_{axis}$ Plg/Azi (°)	45/130
$P_{axis}$ Plg/Azi (°)	45/313
Signal length (s)	300
Weighted reduced variance (%)	88.91
Double couple (%)	91.52
Compensated linear vector dipole (%)	8.48
Quality (after Scognamiglio <i>et al.</i> , 2010)	Aa

### OS fault segment building

To reconstruct the geometry of the fault segments activated by EQ1 and EQ2, referred to as the Paganica fault and the Ocre Segment (OS), respectively (Fig. 3), we adopted a semi-automatic procedure using the Midland Valley MOVE software. Primary data were the Late Quaternary fault traces and fault/slip data

(Lavecchia *et al.*, 2012), the L'Aquila 2009 relocated events (Chiaraluze *et al.*, 2011) and the EQ2 focal mechanism calculated herein. Triangulated fault surfaces were created by interpolating plan-view and section-view fault traces (Fig. S4). The latter were drawn across evident hypocentral alignments and clusters and, whenever possible, were matched to the corresponding outcropping fault.

The built OS fault model allows for a moderate east-dipping surface (average dip  $\sim 45^\circ$ ), which develops at depths between 11 and 16 km beneath the intersection with the SW-dipping Paganica fault. Along strike, the OS extends for  $\sim 15$  km, rotating from WNW (in the north) to NNW (in the south). The OS also shows along-dip variability, with local changes in dip of the triangulated meshes from  $35^\circ$  to  $60^\circ$  (Fig. S4c,d). According to its moment magnitude ( $M_w 5.4$ ), EQ2 would have ruptured an area of  $\sim 6 \times 7$  km<sup>2</sup> (Wells and Coppersmith, 1994) lying on the southern NNW–SSE-striking portion of the OS (Fig. S4c).

### Structural regional context of the OS

We identified the area where the mid-crustal OS might have its surface expression in a Late Quaternary east-dipping extensional system

cropping out in the Sabini-Eastern Simbruini (SES) sector (Fig. 4), along the Latium-Abruzzo regional boundary. In the previous literature, the SES almost exclusively is cut by SW-dipping normal faults (Cosentino *et al.*, 2010; Carminati *et al.*, 2014). In this paper, based on new field observations and fault/slip data synthesized in an updated geological sketch map (Fig. S5), we highlight the systematic presence of high- to moderate-angle ( $60^\circ$ – $40^\circ$ ) NE-dipping normal faults. These faults, which locally bound small asymmetric Late Quaternary continental basins, accommodate a horizontal displacement of  $\sim 1500$  m. Moreover, the interpretation of a short commercial seismic line perpendicular to the SES (1-84-CC-3, Videpi Project, 2016) helps, in spite of the poor quality of the seismic image (Fig. S6), to highlight an east-dipping basal detachment. This detachment is traceable from the surface to  $\sim 2.5$  s TWT ( $\sim 6.7$  km) and delimits the high-angle east- and west-dipping extensional faults at depth (Fig. S6). A 3D view of the reconstructed SES east-dipping geometry is given in the block diagram of Fig. 4b.

With the aim of investigating the possibility of a geometric–kinematic compatibility between the SES and the OS, we constructed a regional geological section (A–A' in Figs. 4a

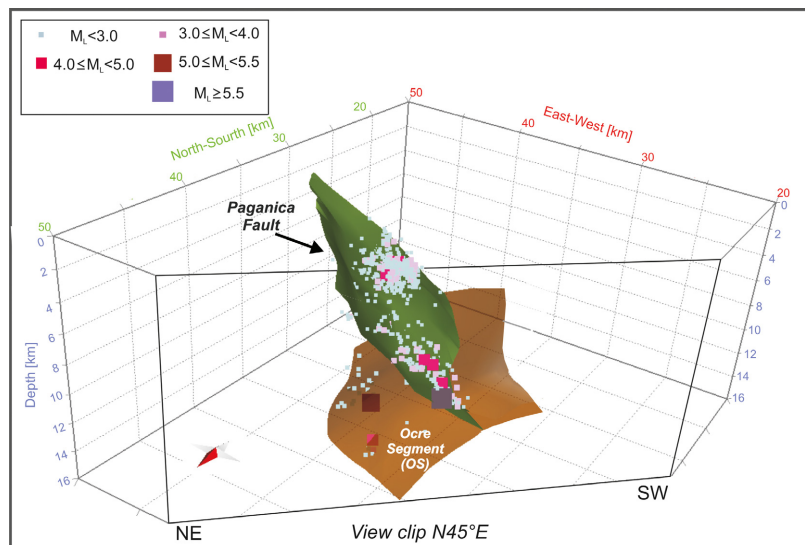


**Fig. 3** 3D model of the fault segments activated by EQ1, EQ2 and their aftershock sequences in the time interval from 6 April to 30 September 2009 (hypocentral data from Chiaraluze *et al.*, 2011). The reconstruction was performed using Move 2016 (Midland Valley academic grant programme). [Colour figure can be viewed at [wileyonlinelibrary.com](http://wileyonlinelibrary.com)]

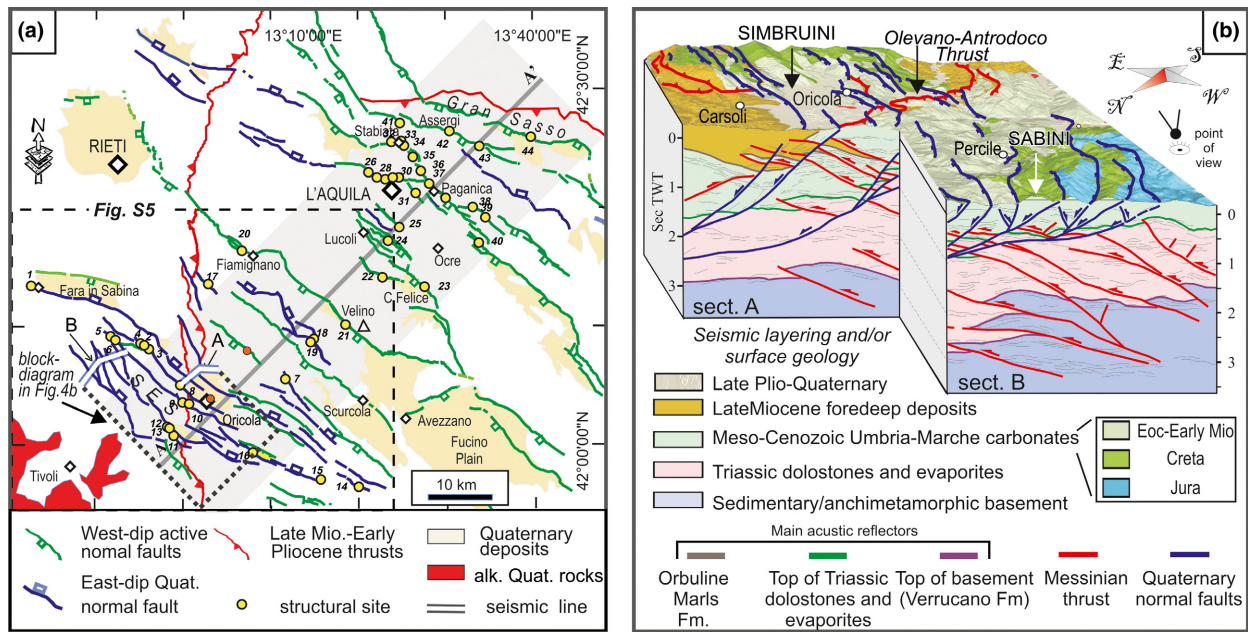


**Fig. 4** (a) Structural map of the Quaternary active fault pattern (location map in Fig. 7b) with fault/slip survey sites (yellow dots), trace of the regional transect (A–A') of Fig. 5a and boundaries (dashed line) of the geological map in Fig. S5. The map was derived from the ARC-GIS fault digital database of the G. Lavecchia research group at DiSPUTer, Ud'A; the west-dipping normal faults are after Boncio *et al.* (2004); the east-dipping ones are new in this paper (see Fig. S5 for geological details). (b) 3D tectonic block diagram of the Sabini-Eastern Simbruini area obtained from the integration of surface geology (Fig. S5) and the geologically interpreted line drawings of two portions (traces A and B in Fig. 4a) of a short commercial seismic line (Fig. S6); the area represented in the block diagram is indicated by a dotted line on the map in Fig. 4a. [Colour figure can be viewed at [wileyonlinelibrary.com](http://wileyonlinelibrary.com)]

and 5a) that extends 85 km in the SW–NE direction, e.g. parallel to the extensional tectonic direction. East of the SES, the section crosses the Quaternary Intra-Apennine Fault System (IAFS). The IAFS consists of moderately steep ( $\sim 45^\circ$ – $70^\circ$  dip angle) west-dipping normal faults. They have been contemporaneously active in Holocene times, but nucleated progressively eastward over time, starting from the Early Pleistocene (Carminati *et al.*, 2014). They accommodate a cumulative net extension of  $\sim 6000$  m with an average strain rate of  $\sim 2.5 \text{ mm a}^{-1}$ .

New fault slip data collected in the SES and in the IAFS were projected along the section trace and, for completeness, integrated with some of our previous data (Ferrarini *et al.*, 2015).

The SES and IAFS geological stress tensors were separately calculated using the inversion procedure proposed in Delvaux and Sperner (2003) (Fig. 5b). A normal-fault regime with a sub-horizontal and  $\sim$ SW–NE-

trending  $\sigma_3$  axis was obtained for both (Table 2). A co-axial tensional seismological stress tensor was also computed for the L'Aquila 2009 sequence, integrating the EQ2 focal solution computed in this study with a focal mechanism dataset ( $M_w \geq 3.5$ ) available in the literature (Herrmann *et al.*, 2011).

The inversion results show the coaxiality among the stress tensors computed for the outcropping east-dipping SES and west-dipping IAFS and for the fault system activated at depth during the L'Aquila seismic sequence (Table 2). The inversion procedure highlights a very small misfit angle ( $8^\circ$ ) between the input EQ2 slip vector and the resolved shear stress on the EQ2 east-dipping preferential seismic plane. In addition, the analysis of slip vector vs. the stress ratio  $\Phi$  (Angelier, 1994) shows that the EQ2 resolved shear stress falls in the range of predicted values (Fig. S7). This implies that the relevant strike-slip component characterizing EQ2 (rake  $\sim 35^\circ$ ) is

kinematically compatible with the L'Aquila 2009 tensional tensor, possibly due to the activation of a pre-existing, nearly N–S-striking plane.

## OS potential fault activity

To investigate the likelihood of the OS being reactivated within the reconstructed stress field, we calculated its slip tendency (*sensu* Morris *et al.*, 1996), expressed as  $T = T_s / T_{s_{\max}}$ , where  $T_s$  is the shear to normal stress ratio and  $T_{s_{\max}}$  is the maximum calculated  $T_s$ . Starting from the reconstructed OS fault model (Figs. 3 and S4) and the seismologic stress tensor attitude (Table 2), we calculated the slip tendency on each OS mesh (Fig. 6). We assumed  $\sigma_1$  equal to the lithostatic pressure ( $\rho_r g z$ ), where  $\rho_r$  was related to the different stratigraphic horizons (cross-section in Fig. 7a). We derived  $\sigma_3$  from the differential stress ( $\sigma_1 - \sigma_3$ ) (Sibson, 1974) at the hypocentral depth of the OS (14 km) and  $\sigma_2$  from the calculated stress ratio

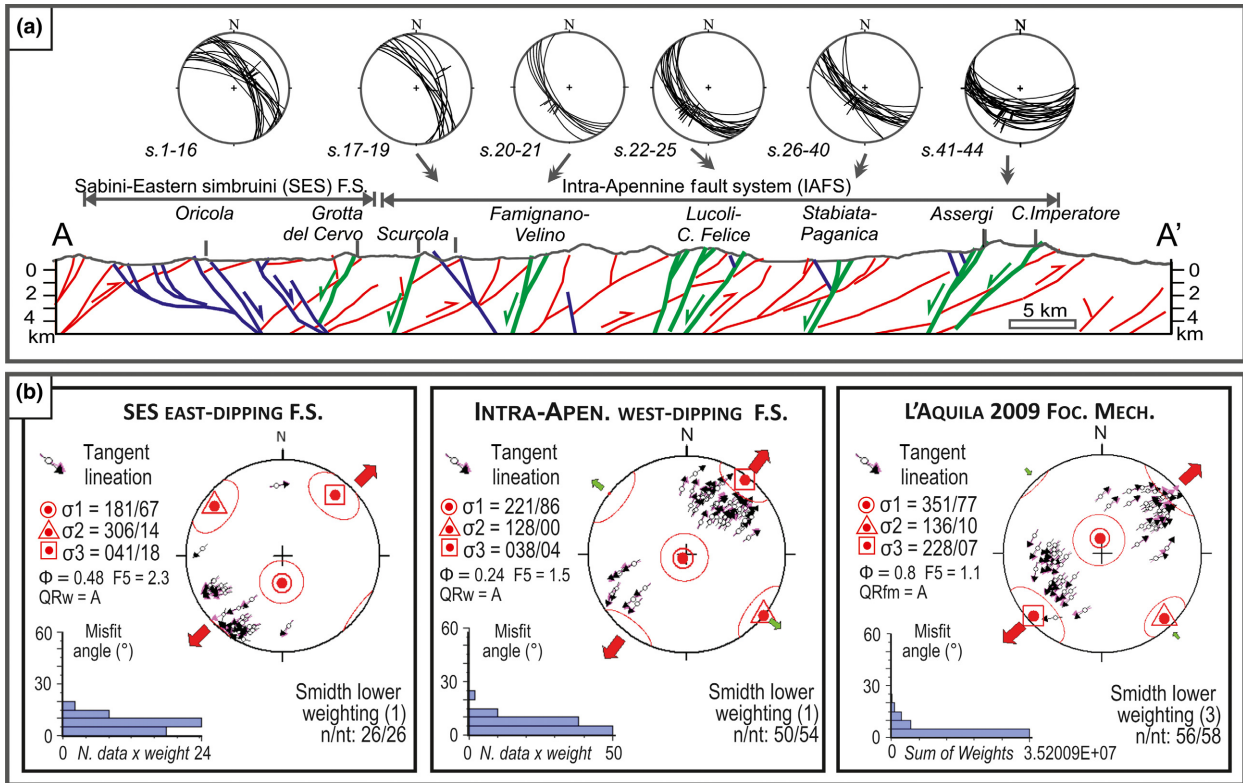


**Fig. 5** (a) Shallow section across the intra-Apennine active extensional system showing the pre-existing thrust structures derived from a geological transect that was originally drawn by the authors at a scale of 1:100,000 (trace in Fig. 4a); the stereonets (Schmidt, lower hemisphere) represent fault slip data at the yellow sites in Fig. 4a (structural sites 1–25 refer to original data in this paper, and sites 26–44 are from Ferrarini *et al.*, 2015). (b) Stress inversion of the geological fault/slip data in Fig. 5a and of the L’Aquila 2009 fault plane solutions (EQ2 focal solution computed in this study, and focal mechanisms for events with  $M_W \geq 3.5$  from Herrmann *et al.*, 2011). Inversion procedure as in Delvaux and Sperner (2003). Key: dark and pink arrows = measured slip directions and resolved shears, respectively (the corresponding misfit angles vs. the number of data points are represented in the histograms); nt = total number of data (e.g. plane/slikenline pairs); n = number of successfully inverted data;  $\sigma_1$ ,  $\sigma_2$ ,  $\sigma_3$  = principal stress axes;  $\Phi$  = stress ratio =  $(\sigma_2 - \sigma_3) / (\sigma_1 - \sigma_3)$ ; QR = quality ranking factors (QR) and the stress inversion parameters with associated uncertainties are listed in Table 2. [Colour figure can be viewed at wileyonlinelibrary.com]

**Table 2** Geological and seismological stress tensor parameters calculated in Fig. 5b for the SES (Sabini-Eastern Simbruini) and IAP (Intra-Apennines) fault systems and for the L’Aquila 2009 sequence. nt = total number of data (e.g., plane/slikenline pairs); n = inverted data;  $\sigma_1$ ,  $\sigma_2$ ,  $\sigma_3$  = principal stress axes;  $\Phi$  = stress ratio =  $(\sigma_2 - \sigma_3) / (\sigma_1 - \sigma_3)$ ; QR = quality ranking: A-QRw as in Sperner *et al.* (2003) and A-QRfm as in Heidbach *et al.* (2010).

Data type	Data (n/nt)	$\sigma_1$	$\pm 1\sigma$	$\sigma_2$	$\pm 1\sigma$	$\sigma_3$	$\pm 1\sigma$	$\Phi$	$\pm 1\sigma$	QR
SES fault/slip	26/26	181/67	18.3	306/14	19.7	041/18	19.7	0.48	0.23	A-QRw
IAP fault/slip	50/54	221/86	19.7	128/00	19.1	038/04	17.6	0.24	0.16	A-QRw
Focal mech.	53/58	351/77	21.2	136/10	15.5	228/07	21.8	0.8	0.41	A-QRfm

( $\sigma_2 = 0.8\sigma_1$ ). We assumed a frictional strength consistent with normal tectonics (Collettini and Sibson, 2001), a hydrostatic fluid regime and cohesionless fault surfaces. Input data and results are given in Table 3 and Fig. 4b. Under such conditions, the OS meshes with dips  $> \sim 30^\circ$  show a

good mechanical tendency to be reactivated under the present stress field ( $T \geq 0.6$ ). Conversely, reactivation is not expected ( $T \leq 0.5$ ) on the low-angle OS meshes ( $< \sim 25^\circ$ ). This stress state is represented well in the Mohr circle in Fig. 6b, where the straight line represents the limiting friction line

that separates the favourably (red to pinkish) and unfavourably (green to bluish) oriented domains. If supra-hydrostatic conditions were assumed, as proposed by Di Luccio *et al.* (2010), a larger portion of the OS would be capable of undergoing seismogenic slip.

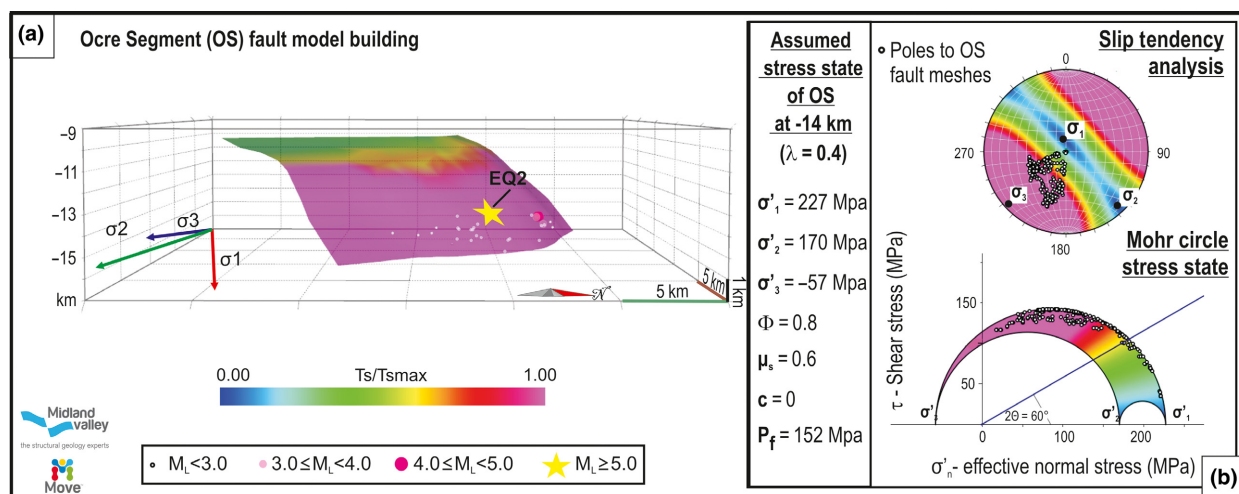


**Fig. 6** (a) 3D fault model of the Ocre Segment, with slip tendency analysis according to Morris *et al.* (1996). (b) Stress state computed with the stress module in the Midland Valley MOVE software; input data as in Table 3. The colour scale represents the likelihood of the OS being activated according to the performed slip tendency analysis. The Mohr circle shows the stress condition of any triangulated OS fault meshes; the straight line represents the limiting friction line (for  $c = 0$  and  $\mu = 0.6$ ) separating favourably (red to pinkish) and unfavourably (green to bluish) oriented domains. [Colour figure can be viewed at [wileyonlinelibrary.com](http://wileyonlinelibrary.com)]

### Proposed model and conclusions

The results provided in this paper support the following observations:

- 1 seismological evidence of a moderate-to-steep ( $35^\circ$ – $60^\circ$ ) east-dipping normal-oblique fault segment, the OS, located at mid-crustal depth beneath the Paganica fault and partially activated by EQ2 (Figs 2, 3 and S4);
- 2 geological evidence of previously under-evaluated moderately east-dipping ( $40^\circ$ – $60^\circ$ ) extensional structures cropping out within the SES and propagating down-dip to depths of 9–10 km (Figs. 4, S5 and S6);
- 3 geological and seismological kinematic compatibility of the SES with the intra-Apennine west-dipping faults (IAFS) and with the L'Aquila focal mechanisms under a common tensional stress field with a SW–NE-trending least-stress axis (Fig. 5);
- 4 no evidence of any transcurrent stress regime at the EQ2 hypocentral depth, but rather evidence of a tensional regime with a SW–NE-trending least-stress axis that can activate favourably oriented pre-existing planes, although with a considerable oblique component (Fig. S7);
- 5 the likelihood of the entire OS being potentially seismogenic

within the reconstructed stress field (Fig. 6).

Considering the above points, we wonder whether, similar to the EFS in the northern Apennines (Fig. 1c), the SES and the OS might be connected at depth, being expressions at different structural levels of the same discontinuity, which dips eastward with a ramp–flat–ramp geometry. The IAFS, which includes the Paganica fault responsible for EQ1, would be antithetic to such a structure, here referred to as the Latium-Abruzzo Extensional Detachment (e.g., LAED). This working hypothesis is presented in Fig. 7a, along the trace of the geological section of Fig. 5a.

The proposed LAED geometry is subdivided into four sectors with different degrees of interpretation and data constraints. Sectors I and IV extend across the western (shallow) and eastern (deep) LAED ramps, respectively, and are constrained by geological and seismological data discussed in this paper (Figs 3–5, S5 and S6).

Sectors II and III extend across the central LAED flat that connects the two lateral ramps, possibly developing at the interface between the Middle Triassic quartzites and phylites and the underlying Late Palaeozoic–Early Triassic low-grade

metamorphic basement (Fig. 7a). The western half of the LAED flat (sector II) is model-driven due to the lack of instrumental activity. The eastern half of the LAED flat (sector III) is inferred from the depth distribution of the background seismicity from 2004 to 2012, which shows a sharp cut-off at  $\sim 10$  km (Bagh *et al.*, 2007; Chiarabba *et al.*, 2015). A sub-horizontal flat behind the Paganica fault is also hypothesized by Atzori *et al.* (2013), based on the interpretation of an anomalous far-field interferometric signal that preceded the 2009 L'Aquila sequence. On the same flat, Borghi *et al.* (2016) located a precursory  $M_w 5.9$  slow-slip seismic event that occurred on 12 February 2009. Furthermore, the presence of an east-dipping low-angle discontinuity at the base of the SW-dipping intra-Apennine seismogenic master fault is highlighted by preliminary aftershock locations of the 2016 Central Italy seismic sequence (Michele *et al.*, 2016) (Fig. 7d).

According to our interpretation, the LAED would represent a regional right-lateral en echelon arm of the Etrurian Fault System (EFS) (Fig. 7b,c). Like the EFS, it would delimit at the base of the intra-Apennine crustal volume undergoing active extension (Fig. 7a). Unlike the EFS breakaway zone, where Late

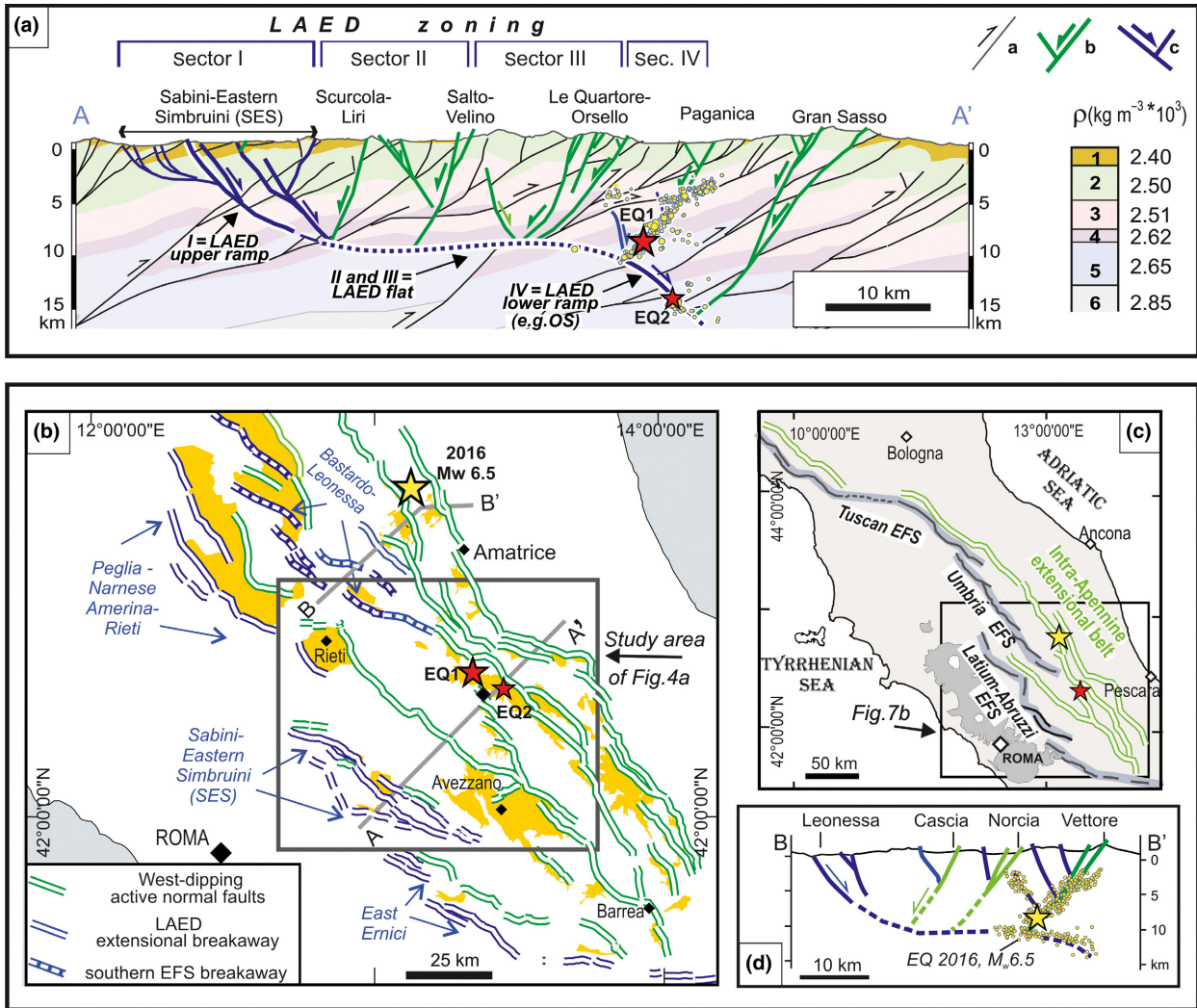


**Fig. 7** Regional seismotectonic framework of the L'Aquila 2009 sequence and structural style of the Quaternary extensional tectonics. (a) Depth interpretation of the transect in Fig. 5a with the hypocentral distribution of the 2009 L'Aquila events relocated by Chiaraluce *et al.* (2011), assuming a half-width of 5 km. Key for the stratigraphic sequence (after Patacca *et al.* (2008) and Cosentino *et al.* (2010)): 1 = Late Miocene siliciclastic foredeep deposits (average thickness 2000 m); 2 = Jurassic–Cretaceous to Early Miocene carbonates (up to 3500–4000 m); 3 = Late Triassic dolostone and evaporites (up to 3000 m); 4 = Middle Triassic quartzites and phyllites (~1500 m); 5 = Late Palaeozoic–Early Triassic low-grade metamorphic basement (average thickness 6000 m); 6 = Middle Palaeozoic crystalline basement; the  $\rho$  density values are from Boncio *et al.* (2004). Key for fault structures: a = Late Miocene–Early Pliocene thrust faults; b and c = east- and west-dipping normal fault systems with associated antithetic faults; LAED = Latium-Abruzzo Extensional Detachment, subdivided into four sectors with different quality rankings in the depth interpretation. (b) Sketch map of the east-dipping Latium-Abruzzo Extensional System and of the antithetic intra-Apennine west-dipping faults as reconstructed in this paper. The red stars represent the epicentres of the two major events ( $M_w$  6.3 and 5.4) of the L'Aquila sequence 2009. The yellow star locates the major event of the Central Italy 2016 seismic sequence (30 September,  $M_w$  6.5). (c) Map highlighting the regional right-lateral en echelon segmentation pattern of the major east-dipping extensional fault systems (EFS) that crop out along the inner border of the seismogenic intra-Apennine extensional domain (modified from Lavecchia *et al.*, 2011). They are here identified as the Tuscan EFS, Umbria EFS and Latium-Abruzzo EFS; the SES, first highlighted in this paper, belongs to the newly defined Latium-Abruzzo Extensional Detachment (LAED). (d) Sketch of the fault pattern along a section that extends across the 2016 Central Italy seismic sequence (trace B–B' in Fig. 7b) (after Lavecchia *et al.*, 2016). The aftershock sequence recorded from 25 August to 15 September 2016 (yellow dots) is from section 1 in Bonini *et al.* (2016). Note that the aftershock sequence reveals both a high-angle west-dipping master fault, where the main event nucleated, and a low-angle east-deepening basal plane, closely recalling the geometry and structural style proposed in this paper for the LAED. [Colour figure can be viewed at [wileyonlinelibrary.com](http://wileyonlinelibrary.com)]

**Table 3** Rock properties and stress conditions computed for the Ocre Segment (reference depth 14 km) and adopted for the slip tendency calculation in Fig. 6.

Rock properties	Values	References
Frictional strength, $\mu$	0.6	Collettini and Sibson (2001)
Cohesion, $c$	0	
Pore fluid factor, $\lambda = P_f/\rho g z$	0.4 (hydrostatic fluid pressure state)	Sibson (2000)
Density, $\rho$ ( $\text{kg m}^{-3} \cdot 10^3$ )	as given in Fig. 7a	This paper
Stress ratio $\Phi = (\sigma_2 - \sigma_3)/(\sigma_1 - \sigma_3)$	0.8	This paper
Stress magnitudes (MPa) $\sigma_1, \sigma_2, \sigma_3$	379, 322, 95	This paper
Effective stress magnitudes (MPa) $\sigma'_1, \sigma'_2, \sigma'_3$	227, 170, -57	This paper
Fluid pressure (MPa) $P_f$	152	This paper

Miocene flysch terranes are juxtaposed against Triassic evaporites (Brozzetti *et al.*, 2009), the tectonic elision cropping out along the LAED breakaway zone, e.g., the SES, is limited to the contact between Early Cretaceous and Early Jurassic formations (Figs. S5 and S6). Nevertheless, we advance the hypothesis that, at depth, the LAED might accrue significant normal-sense displacement, coupled with slip on the synthetic SES and with the progressive eastward shift and extension of the hangingwall volume cross-cut by the IAFS (Fig. S8).

Although the LAED seismogenic role is questionable, preliminary results obtained in this paper (e.g. EQ2/fault association and slip tendency analysis) suggest the possible occurrence of small/moderate (M 4.5–5.5) extensional earthquakes on mid-crustal LAED segments with dip  $>45^\circ$  (Fig. 6). As in the L'Aquila 2009 case, these mid-crustal events might be triggered by major upper-crustal earthquakes on the antithetic high-angle faults, due to stress transfer (De Natale *et al.*, 2011; Serpelloni *et al.*, 2012) and/or fluid migration (Doglioni *et al.*, 2014).

The hypothesis of a regional low-angle east-dipping normal fault beneath the central Apennines might be relevant to the definition of the active extensional style in the region, with consequent implications for seismic hazard evaluations. In addition, the data and interpretation provided in this paper might contribute to the worldwide discussion on the

geometry, kinematics and seismogenic behaviour of continental extensional detachments (Axen, 1999).

### Acknowledgements

This work was financed by DiSPUTer, University of Chieti “G. d’Annunzio” (research funding to Giusy Lavecchia) and by the Department of Physics, University of Naples “Federico II” (research funding to Aldo Zollo). The 3D fault modelling and slip tendency analysis were performed using the Move Software Suite 2016, which was granted by Midland Valley’s Academic Software Initiative. We thank Lauro Chiaraluce for providing the relocated L'Aquila 2009 dataset and Martin Vallée for the source code that was used to compute the ASTFs. Many thanks also to the Terra Nova editor, Carlo Doglioni, and to Massimiliano Barchi and an anonymous referee for their criticism and helpful suggestions. The data are listed in the references, tables and supplements.

### References

- Adinolfi, G.M., De Matteis, R., Orefice, A., Festa, G., Zollo, A., de Nardis, R. and Lavecchia, G., 2015. The September 27, 2012, M<sub>L</sub> 4.1, Benevento earthquake: a case of strike-slip faulting in Southern Apennines (Italy). *Tectonophysics*, **660**, 35–46. doi:10.1016/j.tecto.2015.06.036.
- Amato, A. and Mele, F., 2008. Performance of the INGV National Seismic Network from 1997 to 2007. *Ann. Geophys.*, **51**, 417–431.
- Angelier, J., 1994. Fault slip analysis and paleostress reconstruction. In: *Continental Deformation* (P.L.

Hancock, ed), pp. 417–431. Pergamon Press Ltd, Oxford.

- Atzori, S., Chiarabba, C., Devoti, R., Bonano, M. and Lanari, R., 2013. Anomalous far-field geodetic signature related to the 2009 L'Aquila (central Italy) earthquake. *Terra Nova*, **25**, 343–351.
- Axen, G.J., 1999. Low-angle normal fault earthquakes and triggering. *Geophys. Res. Lett.*, **26**, 3693–3696.
- Bagh, S., Chiaraluce, L., De Gori, P., Moretti, M., Govoni, A., Chiarabba, C., Di Bartolomeo, P. and Romanelli, M., 2007. Background seismicity in the Central Apennines of Italy: the Abruzzo region case study. *Tectonophysics*, **444**, 80–92.
- Barchi, M., De Feyter, A., Magnani, M., Minelli, G., Piali, G. and Sotera, B., 1998. Extensional tectonics in the Northern Apennines (Italy): evidence from the CROP03 deep seismic reflection line. *Mem. Soc. Geol. Ital.*, **52**, 528–538.
- Boncio, P., Brozzetti, F. and Lavecchia, G., 2000. Architecture and seismotectonics of a regional low-angle normal fault zone in central Italy. *Tectonics*, **19**, 1038–1055.
- Boncio, P., Lavecchia, G. and Pace, B., 2004. Defining a model of 3D seismogenic sources for Seismic Hazard Assessment applications: the case of central Apennines (Italy). *J. Seismol.*, **8**, 407–425.
- Boncio, P., Pizzi, A., Brozzetti, F., Pomposo, G., Lavecchia, G., Di Naccio, D. and Ferrarini, F., 2010. Coseismic ground deformation of the 6 April 2009 L'Aquila earthquake (central Italy, M<sub>w</sub> 6.3). *Geophys. Res. Lett.*, **37**, L06308, doi:10.1029/2010GL042807.
- Bonini, L., Maesano, F.E., Basili, R., Burrato, P., Carafa, M.M.C., Fracassi, U., Kastelic, V., Tarabusi, G., Tiberti, M.M., Vannoli, P. and Valensise, G., 2016. Imaging the tectonic framework of the 24 August 2016, Amatrice (central Italy) earthquake sequence: new roles for old players? *Ann. Geophys.*, **59**, FAST TRACK 5, DOI: 10.4401/ag-7229.
- Borghesi, A., Aoudia, A., Javed, F. and Barzaghi, R., 2016. Precursory slow-slip loaded the 2009 L'Aquila earthquake sequence. *Geophys. J. Int.*, **205**, 776–784.
- Brozzetti, F., 2011. The Campania-Lucania Extensional Fault System, southern Italy: a suggestion for a uniform model of active extension in the Italian Apennines. *Tectonics*, **30**, TC5009, doi:10.1029/2010TC002794.
- Brozzetti, F., Boncio, P., Lavecchia, G. and Pace, B., 2009. Present activity and seismogenic potential of a low-angle

- normal fault system (Città di Castello, Italy): constraints from surface geology, seismic reflection data and seismicity. *Tectonophysics*, **463**, 31–46.
- Carminati, E., Fabbi, S. and Santantonio, M., 2014. Slab bending, syn-subduction normal faulting, and out-of-sequence thrusting in the Central Apennines. *Tectonics*, **33**, 530–551.
- Chiarabba, C., De Gori, P. and Mele, F.M., 2015. Recent seismicity of Italy: active tectonics of the central Mediterranean region and seismicity rate changes after the  $M_w$  6.3 L'Aquila earthquake. *Tectonophysics*, **638**, 82–93.
- Chiaraluca, L., Chiarabba, C., Collettini, C., Piccinini, D. and Cocco, M., 2007. Architecture and mechanics of an active low-angle normal fault: Alto Tiberina Fault, northern Apennines, Italy. *J. Geophys. Res.*, **112**, B10310. doi:10.1029/2007JB005015.
- Chiaraluca, L., Valoroso, L., Piccinini, D., Di Stefano, R. and De Gori, P., 2011. The anatomy of the 2009 L'Aquila normal fault system (central Italy) imaged by high resolution foreshock and aftershock locations. *J. Geophys. Res. B: Solid Earth*, **116**, B12311, doi:10.1029/2011JB008352.
- Collettini, C. and Sibson, R.H., 2001. Normal faults, normal friction? *Geology*, **29**, 927–930.
- Collettini, C., De Paola, N., Holdsworth, R.E. and Barchi, M.R., 2006. The development and behaviour of low-angle normal faults during Cenozoic asymmetric extension in the Northern Apennines, Italy. *J. Struct. Geol.*, **28**, 333–352.
- Cosentino, D., Cipollari, P., Marsili, P. and Scrocca, D., 2010. Geology of the central Apennines: a regional review. In: *The Geology of Italy, 2010* (M. Beltrando, A. Peccerillo, M. Mattei, S. Conticelli and C. Doglioni, eds.). *J. Virtual Explor.*, Electronic Edition, ISSN 1441-8142, **36**, paper 12, doi: 10.3809/jvirtex.2010.00223.
- D'Amico, S., Orecchio, B., Presti, D., Neri, G., Wu, W., Sandu, I., Zhu, L. and Herrmann, R.B., 2013. Source parameters of small and moderate earthquakes in the area of the 2009 L'Aquila earthquake sequence (central Italy). *Phys. Chem. Earth*, **63**, 77–91.
- De Matteis, R., Matrullo, E., Rivera, L., Stabile, T.A., Pasquale, G. and Zollo, A., 2012. Fault delineation and regional stress direction from the analysis of background microseismicity in the southern Apennines, Italy. *Bull. Seismol. Soc. Am.*, **102**, 1899–1907.
- De Natale, G., Crippa, B., Troise, C. and Pingue, F., 2011. Abruzzo, Italy, earthquakes of April 2009: heterogeneous fault-slip models and stress transfer from accurate inversion of ENVISAT-InSAR data. *Bull. Seismol. Soc. Am.*, **101**, 2340–2354.
- Delvaux, D. and Sperner, B., 2003. New aspects of tectonic stress inversion with reference to the TENSOR program. In: *New Insights into Structural Interpretation and Modelling* (D.A. Nieuwland, ed.). *J. Geol. Soc. London Spec. Publ.*, **212**, 75–100.
- Di Luccio, F., Ventura, G., Di Giovambattista, R., Piscini, A. and Cinti, F.R., 2010. Normal faults and thrusts reactivated by deep fluids: the 6 April 2009  $M_w$  6.3 L'Aquila earthquake, central Italy. *J. Geophys. Res. B: Solid Earth*, **115**, B06315, doi:10.1029/2009JB007190.
- Di Luzio, E., Mele, G., Tiberti, M.M., Cavinato, G.P. and Parotto, M., 2009. Moho deepening and shallow upper crustal delamination beneath the central Apennines. *Earth Planet. Sci. Lett.*, **280**, 1–12.
- Di Naccio, D., Boncio, P., Brozzetti, F., Pazzaglia, F.J. and Lavecchia, G., 2013. Morphotectonic analysis of the Lunigiana and Garfagnana grabens (northern Apennines, Italy): implications for active normal faulting. *Geomorphology*, **201**, 293–311.
- Doglioni, C., Harabaglia, P., Merlini, S., Mongelli, F., Peccerillo, A.T. and Piromallo, C., 1999. Orogens and slabs vs. their direction of subduction. *Earth Sci. Rev.* **45**, 167–208.
- Doglioni, C., Barba, S., Carminati, E. and Riguzzi, F., 2011. Role of the brittle-ductile transition on fault activation. *Phys. Earth Planet. Int.*, **184**, 160–171.
- Doglioni, C., Barba, S., Carminati, E. and Riguzzi, F., 2014. Fault on-off versus coseismic fluids reaction. *Geosci. Front.*, **5**, 767–780. doi:doi.org/10.1016/j.gsf.2013.08.004.
- Dreger, D.S., 2003. 85.11 TDMT\_INV: time domain seismic moment tensor INVersion. *Int. Geophys.*, **81**, 1627.
- Dreger, D.S. and Helmberger, D.V., 1993. Determination of source parameters at regional distances with three-component sparse network data. *J. Geophys. Res. B: Solid Earth*, **98**(B5), 8107–8125.
- Eva, E., Solarino, S. and Boncio, P., 2014. HypoDD relocated seismicity in northern Apennines (Italy) preceding the 2013 seismic unrest: seismotectonic implications for the Lunigiana-Garfagnana area. *B. Geofis. Teor. Appl.*, **55**, 739–754.
- Ferrari, F., Lavecchia, G., de Nardis, R. and Brozzetti, F., 2015. Fault geometry and active stress from earthquakes and field geology data analysis: the Colfiorito 1997 and L'Aquila 2009 cases (Central Italy). *Pure Appl. Geophys.*, **172**, 1079–1103.
- Festa, G. and Zollo, A., 2006. Fault slip and rupture velocity inversion by isochrones back projection. *Geophys. J. Int.*, **166**, 745–756.
- Galadini, F. and Galli, P., 2000. Active tectonics in the central Apennines (Italy) - input data for seismic hazard assessment. *Nat. Hazards*, **22**, 225–270.
- Galli, P. and Peronace, E., 2014. New paleoseismological data from the Irpinia fault. A different seismogenic perspective for the southern Apennines. *Earth Sci. Rev.*, **136**, 175–201.
- Ghisetti, F. and Vezzani, L., 2002. Normal faulting, transcrustal permeability and seismogenesis in the Apennines (Italy). *Tectonophysics*, **348**, 155–168.
- Gorini, A., Nicoletti, M., Marsan, P., Bianconi, R., De Nardis, R., Filippi, L., Marcucci, S., Palma, F. and Zambonelli, E., 2010. The Italian strong motion network (2010). *Bull. Earthq. Eng.*, **8**, 1075–1090.
- Guglielmino, F., Anzidei, M., Briole, P., Elias, P. and Puglisi, G., 2013. 3D displacement maps of the 2009 L'Aquila earthquake (Italy) by applying the SISTEM method to GPS and DInSAR data. *Terra Nova*, **25**, 79–85.
- Hartzell, S.H., 1978. Earthquake aftershocks as Green's functions. *Geophys. Res. Lett.*, **5**, 1–4.
- Heidbach, O., Tingay, M., Barth, A., Reinecker, J., Kurfeß, D. and Müller, B., 2010. Global crustal stress pattern based on the World Stress Map database release 2008. *Tectonophysics*, **482**, 3–15.
- Herrmann, R.B., Malagnini, L. and Munafò, I., 2011. Regional moment tensors of the 2009 L'Aquila earthquake sequence. *Bull. Seismol. Soc. Am.*, **101**, 975–993.
- Lavecchia, G., Brozzetti, F., Barchi, M., Menichetti, M. and Keller, J.V., 1994. Seismotectonic zoning in east-central Italy deduced from an analysis of the Neogene to present deformations and related stress fields. *Geol. Soc. Am. Bull.*, **106**, 1107–1120.
- Lavecchia, G., Boncio, P., Brozzetti, F., de Nardis, R., Di Naccio, D., Ferrarini, F., Pizzi, A. and Pomposo, G., 2011. The April 2009 L'Aquila (central Italy) seismic sequence ( $M_w$ 6.3): a preliminary seismotectonic picture. In: *Recent Progress on Earthquake Geology* (P. Guarnieri, ed.), pp. 1–17. Nova Science Publishers, New York.
- Lavecchia, G., Ferrarini, F., Brozzetti, F., de Nardis, R., Boncio, P. and Chiaraluca, L., 2012. From surface geology to aftershock analysis: constraints on the geometry of the

- L'Aquila 2009 seismogenic fault system. *Ital. J. Geosci.*, **131**, 330–347.
- Lavecchia, G., Castaldo, R., de Nardis, R., De Novellis, V., Ferrarini, F., Brozzetti, F., Solaro, G., Cirillo, D., Bonano, M., Boncio, P., Casu, F., De Luca, C., Lanari, R., Manunta, M., Manzo, M., Pepe, A., Zinno, I. and Tizzani, P., 2016. Ground deformation and source geometry of the August 24, 2016 Amatrice earthquake (Central Italy) investigated through analytical and numerical modeling of DInSAR measurements and structural-geological data. *Geophys. Res. Lett.*, **43**, DOI:10.1002/2016GL071723
- Maschio, L., Ferranti, L. and Burrato, P., 2005. Active extension in Val d'Agri area, Southern Apennines, Italy: implications for the geometry of the seismogenic belt. *Geophys. J. Int.*, **162**, 591–609.
- Michele, M.R., Di Stefano, L., Chiaraluze, M., Cattaneo, P., De Gori, G., Monachesi, D., Latorre, S., Marzorati, L., Valeroso, C., Ladina, C., Chiarabba, Lauciani, V. and Fares, M., 2016. The Amatrice 2016 seismic sequence: a preliminary look to the mainshock and aftershocks distribution. *Ann. Geophys.*, **59**, Fast Track 5; DOI:10.4401/ag-7227
- Mirabella, F., Brozzetti, F., Lupattelli, A. and Barchi, M.R., 2011. Tectonic evolution of a low-angle extensional fault system from restored cross-sections in the Northern Apennines (Italy). *Tectonics*, **30**, TC6002, doi:10.1029/2011TC002890.
- Morris, A., Ferrill, D.A. and Henderson, D.B., 1996. Slip-tendency analysis and fault reactivation. *Geology*, **24**, 275–278.
- Pace, P., Peruzza, L., Lavecchia, G. and Boncio, P., 2006. Layered Seismogenic Source Model and Probabilistic Seismic-Hazard Analyses in Central Italy. *Bull. Seismol. Soc. Am.*, **96**, 107–132.
- Patacca, E., Scandone, P., Di Luzio, E., Cavinato, G.P. and Parotto, M., 2008. Structural architecture of the central Apennines: interpretation of the CROP 11 seismic profile from the Adriatic coast to the orographic divide. *Tectonics*, **27**, TC3006. doi:10.1029/2005TC001917.
- Petricca, P., Barba, S., Carminati, E., Doglioni, C. and Riguzzi, F., 2015. Gravitational quakes in Italy. *Tectonophysics*, **656**, 202–214. doi:10.1016/j.tecto.2015.07.001.
- Pino, N.A. and Di Luccio, F., 2009. Source complexity of the 6 April 2009 L'Aquila (central Italy) earthquake and its strongest aftershock revealed by elementary seismological analysis. *Geophys. Res. Lett.*, **36**, L23305, doi:10.1029/2009GL041331.
- Pondrelli, S., Salimbeni, S., Morelli, A., Ekström, G., Olivieri, M. and Boschi, E., 2010. Seismic moment tensors of the April 2009, L'Aquila (Central Italy), earthquake sequence. *Geophys. J. Int.*, **180**, 238–242.
- Roberts, G.P. and Michetti, A.M., 2004. Spatial and temporal variations in growth rates along active normal fault systems: an example from the Lazio-Abruzzo Apennines, central Italy. *J. Struct. Geol.*, **26**, 339–376.
- Rovida, A., Camassi, R., Gasperini, P. and Stucchi, M. (eds.), 2011. CPTI11, the 2011 version of the Parametric Catalogue of Italian Earthquakes. Istituto Nazionale di Geofisica e Vulcanologia, Milano, Bologna. Available at: <http://emidius.mi.ingv.it/CPTI11/>.
- Saikia, C.K., 1994. Modified frequency-wavenumber algorithm for regional seismograms using Filon's quadrature: modelling of Lg waves in eastern North America. *Geophys. J. Int.*, **118**, 142–158.
- Scognamiglio, L., Tinti, E., Michelini, A., Dreger, A.S., Cirella, A., Cocco, M., Mazza, S. and Piatanesi, A., 2010. Fast determination of moment tensors and rupture history: what has been learned from the 6 April 2009 L'Aquila earthquake sequence. *Seismol. Res. Lett.*, **81**, 892–906.
- Serpelloni, E., Anderlini, L. and Belardinelli, M.E., 2012. Fault geometry, coseismic-slip distribution and Coulomb stress change associated with the 2009 April 6,  $M_w$  6.3, L'Aquila earthquake from inversion of GPS displacements. *Geophys. J. Int.*, **188**, 473–489.
- Sibson, H.R., 1974. Frictional constraints on thrust, wrench and normal faults. *Nature*, **249**, 542–544.
- Sibson, H.R., 2000. Fluid involvement in normal faulting. *J. Geodyn.*, **29**, 469–499.
- Sokos, E.N. and Zahradnik, J., 2008. ISOLA a Fortran code and a Matlab GUI to perform multiple-point source inversion of seismic data. *Comput. Geosci.*, **34**, 967–977.
- Sokos, E. and Zahradnik, J., 2013. Evaluating centroid-moment-tensor uncertainty in the new version of ISOLA software. *Seismol. Res. Lett.*, **84**, 656–665.
- Sperner, B., Müller, B., Heidbach, O., Delvaux, D., Reinecker, J. and Fuchs, K., 2003. Tectonic stress in the Earth's crust: advances in the World Stress Map project. In: *New Insights into Structural Interpretation and Modelling* (D.A. Nieuwland, ed.). *J. Geol. Soc. London Spec. Publ.*, **212**, 101–116.
- Vallée, M., 2004. Stabilizing the empirical Green function analysis: development of the projected Landweber method. *Bull. Seismol. Soc. Am.*, **94**, 394–409.
- Valeroso, L., Chiaraluze, L., Piccinini, D., Di Stefano, R., Schaff, D. and Waldhauser, F., 2013. Radiography of a normal fault system by 64,000 high-precision earthquake locations: the 2009 L'Aquila (central Italy) case study. *J. Geophys. Res. B: Solid Earth*, **118**, 1156–1176.
- VIDEPI Project, 2016. Visibility of Petroleum Exploration Data in Italy, Ministry for Economic Development UNMIG. Available at: [http://unmig.sviluppoeconomico.gov.it/videpi/cessati/sismica\\_titoli.asp](http://unmig.sviluppoeconomico.gov.it/videpi/cessati/sismica_titoli.asp).
- Wells, D.L. and Coppersmith, K.J., 1994. New empirical relationships among magnitude, rupture length, 924 rupture width, rupture area, and surface displacement. *Bull. Seismol. Soc. Am.*, **84**, 974–1002.
- Working Group DISS, 2015. Database of Individual Seismogenic Sources (DISS), Version 3.2.0: A compilation of potential sources for earthquakes larger than  $M$  5.5 in Italy and surrounding areas. Available at: <http://diss.rm.ingv.it/diss/>
- Zambonelli, E., de Nardis, R., Filippi, L., Nicoletti, M. and Dolce, M., 2011. Performance of the Italian strong motion network during the 2009, L'Aquila seismic sequence (central Italy). *Bull. Earthq. Eng.*, **9**, 39–65.
- Zoback, M.L., 1992. First- and second-order patterns of stress in the lithosphere: The World Stress Map Project. *J. Geophys. Res.*, **97**, 11703–11728.

Received 4 May 2016; revised version accepted 23 November 2016

## Supporting Information

Additional Supporting Information may be found in the online version of this article:

**Figure S1.** (a) Centralized National Seismic Network (RSNC) broadband seismic stations (triangles) used in this study for the TDMT inversion. (b) Displacement waveform fit between observed (black lines) and synthetic (red lines) data of the TDMT solution (Dreger and Helmberger, 1993; Dreger, 2003) obtained for EQ2. The seismograms are sorted by increasing source-to-station azimuth ( $\phi$ ); epicentral distance ( $\Delta$ ) and

variance reduction (VR) are also reported. We used broadband velocity waveforms that were recorded at RSNC between 100 km and 400 km from the earthquake epicentre to consider records with good signal-to-noise ratios and to avoid the use of saturated waveforms. The Green's functions were computed with the frequency–wave number integration method (Saikia, 1994) in the 1-D regional velocity model proposed by Herrmann *et al.* (2011). After fixing the depth and the location of the earthquake, we inverted data from 9 stations and obtained a solution with a variance reduction of ~89% and a percentage of double couple (DC) of ~91%.

**Figure S2.** Uncertainty assessment of the source angles and Kagan angle of the calculated TDMT solution (Table 1 of the main document). The uncertainty analysis was performed by calculating the theoretical error ellipsoid for a fixed source position and time as proposed by Sokos and Zahradnik (2013) with ISOLA software (Sokos and Zahradnik, 2008). The source–station configuration, frequency range and crustal model define the ellipsoid shape and orientation, whereas the absolute size of the error ellipsoid is determined by the variance of the data. In each panel, the nodal planes are indicated with red dashed lines and are derived from the moment tensor solution calculated in this study. The grey histograms represent the potential and acceptable solutions, as function of the data variance. The angle values associated with the constrained seismic preferential plane are reported in underlined bold italic. The uncertainty values are small, indicating a well constrained focal mechanism solution. Referring to the preferential seismic plane, (a) the strike value varies between  $347^\circ$  and  $344^\circ$ ; (b) the dip value centred on  $58^\circ$  varies over a range of  $4^\circ$ , whereas (c) the rake ( $-34^\circ$ ) varies mainly between  $-32^\circ$  and  $-34^\circ$ . Moreover, (d) the Kagan angle, that is, the angle between acceptable solutions compared with the optimal solution, shows values whose mean is about  $1^\circ$  with a standard deviation of 0.5. This additional parameter underlines the low uncertainty of the focal mechanism solution.

**Figure S3.** (a) EQ2 slip map obtained by isochrone back-projection computed with a rupture velocity of 1.8 km/s. The ASTFs shapes discriminate the ENE-dipping plane of the computed TDMT focal mechanism (Fig. 2a in the main document) as the one for which the misfit function is minimized (Fig. 2c in the main document). After testing different rupture velocities, we selected the final kinematic model that minimizes the L1-norm between the synthetic and observed ASTFs (Fig. 2b in the main document). The fault geometry was fixed at the solution that is derived from the computed focal mechanism (ENE-dipping plane). We adopted the deconvolution technique that was proposed by Vallée (2004). The deconvolution was performed at 15 stations (Fig. 2a in the main document) for the direct S wave in the frequency range 0.01–2 Hz based on the limits that were imposed by the expected corner frequency of the master event and the stability of the S-wave polarization.

**Figure S4.** (a,b) 3D-model of the Paganica fault segment activated by EQ1 and its aftershock sequences in the time interval from 6 April to 30 September 2009 (dataset from Chiaraluce *et al.*, 2011). To reconstruct the 3D surfaces, we adopted a semi-automatic procedure using the Midland Valley MOVE software (vers.2016). First, we traced closely spaced (1.25 km semi-width) and differently oriented sets of sections across the epicentral area, in the MOVE georeferenced frame. Second, we drew the fault trace connecting the aftershock volume and the surface fault in the MOVE section-view window. Third, we used the Delaunay Triangulation function to build the fault surfaces. The extent of the seismogenic patch activated by the 6 April main shock and by its aftershock sequence with respect to the overall Paganica fault surface is highlighted in Fig. S4b. (c,d) 3D-model of the Ocre Segment (OS) activated by EQ2 and by the other deep events (depth >11 km) of the L'Aquila 2009 sequence. (c) Triangulated meshes of the OS surface reconstructed according to the same work-flow adopted for the Paganica fault in Fig. S4b. The white dashed line is a schematic representation of the EQ2 ( $M_w 5.4$ ) rupture area

calculated according to scale law (about  $6 \times 7$  km from Wells and Coppersmith, 1994). (d) Histograms of the strike and dip of the OS triangulated surfaces, showing the OS along-strike and along-dip variability.

**Figure S5.** Geological map of the Sabini-Eastern Simbruini (SES) and Carseolani Mts. area, simplified from the Carta Geologica d'Italia, 1:100,000 scale, sheets 144–145–150–151 (Servizio Geologico d'Italia; [http://193.206.192.231/carta\\_geologica\\_italia/default.htm](http://193.206.192.231/carta_geologica_italia/default.htm)) and redrawn on a GIS-platform with original field data from the authors. The map is overlain on a 20 m digital elevation model. The structural sites surveyed along the SES normal faults are indicated by yellow dots and numbered from 1 to 19; the corresponding fault/slip data are represented in a number of stereographic plots (Schmidt net, lower hemisphere) as both (a) cyclographic trace/lineation and (b) poles to major normal faults and contouring of the associated slip vectors.

**Figure S6.** Two portions of the commercial seismic line 1-84-CC3 (VIDEPI Project, 2016; <http://unmig.mise.gov.it/deposito/videpi/allegati/1214.pdf>) extending in an average SW–NE direction across the Sabini-Eastern Simbruini (SES) extensional system (traces in Fig. S5), with corresponding line drawing and geological interpretation of the main reflectors and seismic facies. In spite of the generally poor quality of the line, some closely spaced and relatively continuous packages of reflections, separated by areas with low-continuity signals, can be detected and traced along the entire section. Taking into account the outcropping stratigraphic units and fault planes (Fig. S5), the average stratigraphic thickness given in the literature (Patacca *et al.*, 2008; Cosentino *et al.*, 2010) and the corresponding seismic and mechanical stratigraphy (Di Luzio *et al.*, 2009 and references therein), these reflectors can be referred to the tops and the stratigraphic units reported in the legend.

**Figure S7.** Slip vector variability range for the preferential fault plane of the EQ2 focal mechanism (Table 1), in the L'Aquila 2009 computed extensional stress regime (Table 2), as function of the stress ratio  $\Phi$  (after Angelier, 1994). Key:

EQ2 preferential seismic plane as in Fig. 2a;  $n$  = pole to the EQ2 preferential seismic plane;  $\sigma_1$ ,  $\sigma_2$ ,  $\sigma_3$  = principal stress axes as in Table 2;  $\alpha$  = misfit angle between the observed and the optimized slip vector on the EQ2 preferential seismic plane; M-Plane = movement plane, which contains the pole to the fault plane and the slip direction. The extreme positions of the shear stresses, e.g.  $\tau_0$  (for  $\Phi = 0$ , when  $\sigma_2 = \sigma_3$ ) and  $\tau_1$  (for  $\Phi = 1$ , when  $\sigma_2 = \sigma_1$ ), define the slip variability range (as  $\Phi$  increases from 0 to 1), the slip vector being assumed to be parallel to the shear stress. In our specific case, both the EQ2 measured slip vector and the EQ2

resolved shear stress fall within the range of slip variability. Coherently with the calculated stress ratio value ( $\Phi = 0.8$ ) (Table 2), they both place near the  $\tau_1$  value. The reconstructed picture shows that, in spite of its relevant left-lateral strike-slip component, the EQ2 preferential seismic plane is kinematically compatible with the overall L'Aquila 2009 extensional tensor.

**Figure S8.** Sequential steps of off-set accommodation across a schematic section that in its final stage recalls the LAED structural style, e.g. an east-dipping detachment with a double-ramp geometry coupled with antithetic west-dipping high-angle faults. A simple forward

model was built with Move software (Midland Valley, 2016), assuming that the hanging wall faults progressively grew eastward. The diagram helps to highlight the different partitioning of net extension at the surface and at depth. In fact, at the surface the net displacement in the final stage section is accommodated prevalently by high-angle west-dipping faults ( $d_3$ ,  $d_4$ ,  $d_5$ ) and subordinately by the moderately east-dipping ones ( $d_1$ ,  $d_2$ ). At depth, conversely, almost all the displacement ( $d_6$ ) occurs along the basal extensional detachment.